RESEARCH ARTICLE | JULY 13 2023

Localization of fixed dipoles at high precision by accounting for sample drift during illumination

Special Collection: Advances in Optical Microscopy for Bioimaging

Fabian Hinterer ; Magdalena C. Schneider ; Simon Hubmer ; Montserrat López-Martínez; Ronny Ramlau ; Gerhard J. Schütz

Appl. Phys. Lett. 123, 023703 (2023)
https://doi.org/10.1063/5.0137834

Applied Physics Letters ARTICLE pubs.aip.org/aip/apl

Localization of fixed dipoles at high precision by accounting for sample drift during illumination

Cite as: Appl. Phys. Lett. **123**, 023703 (2023); doi: 10.1063/5.0137834
Submitted: 6 December 2022 · Accepted: 28 June 2023 ·
Published Online: 13 July 2023

Fabian Hinterer,[1,a)] Magdalena C. Schneider,[2,3,a)] Simon Hubmer,[4] Montserrat López-Martínez,[2] Ronny Ramlau,[1] and Gerhard J. Schütz[2]

AFFILIATIONS

[1]Johannes Kepler University, Institute of Industrial Mathematics, Linz, Austria
[2]TU Wien, Institute of Applied Physics, Vienna, Austria
[3]Janelia Research Campus, Howard Hughes Medical Institute, Ashburn, Virginia 20147, USA
[4]Johann Radon Institute Linz, Linz, Austria

Note: This paper is part of the APL Special Collection on Advances in Optical Microscopy for Bioimaging.
[a)]**Authors to whom correspondence should be addressed:** fabian.hinterer@indmath.uni-linz.ac.at and schneiderm2@hhmi.org

ABSTRACT

Single molecule localization microscopy relies on the precise quantification of the position of single dye emitters in a sample. This precision is improved by the number of photons that can be detected from each molecule. Particularly recording at cryogenic temperatures dramatically reduces photobleaching and would, hence, in principle, allow the user to massively increase the illumination time to several seconds. The downside of long illuminations, however, would be image blur due to inevitable jitter or drift occurring during the illuminations, which deteriorates the localization precision. In this paper, we theoretically demonstrate that a parallel recording of the fiducial marker beads together with a fitting approach accounting for the full drift trajectory allows for largely eliminating drift effects for drift magnitudes of several hundred nanometers per frame. We showcase the method for linear and diffusional drift as well as oscillations, assuming fixed dipole orientations during each illumination.

Single molecule localization microscopy (SMLM) techniques, including STORM[1,2] and PALM,[3] rely on the temporal separation of the fluorescent emission from dye molecules, resulting in the sequential imaging of only a sparse subset of emitters in each frame. The position of the emitters can then be localized with arbitrary high precision, limited mainly by the signal-to-noise ratio (SNR) of the data. Performing SMLM at cryogenic conditions has been suggested as a useful alternative to room temperature experiments, as it allows for massively improving single molecule localization precision due to increased photon yields and reduced photobleaching.[4,5] However, fully utilizing the advantage of lower photobleaching kinetics requires the application of very long illumination times, during which sample drift might become problematic.

Generally, sample drift poses a challenge for SMLM as it introduces errors in determining the exact position of the single-molecule emitters.[6] Sample drift can be caused by a variety of reasons, such as thermal fluctuations, vibrations, and mechanical instabilities of the setup. While sample motion during image acquisition should be reduced as much as possible, in practice it cannot be prevented completely, especially during the large acquisition times required for (cryo-)SMLM. Additional drift during cryo-SMLM measurements might be caused by thermal gradients or liquid nitrogen bubbling.[7]

One proposed method to compensate for the drift during acquisition is by means of closed feedback loops.[8,9] While this approach is common for correcting axial drift in order to keep the microscope in focus, implementations for lateral drift are rare. Real-time lateral drift compensation requires a dedicated piezoelectric sample stage that requires complex modifications to some microscopy setups. In the case of SMLM at cryogenic temperatures, the sample needs to be mounted on a cryostat, either in direct contact to liquid nitrogen or in a vacuum isolated environment, which, although possible,[10] considerably complicates the implementation of an active drift compensation stage.

Current post-processing drift compensation methods aim at correcting for sample drift occurring between illuminations. They can be grouped into methods that exploit the tracking of fiducial markers[11–13] and cross correlation methods.[14,15] One advantage of cross correlation methods is that they can be applied without the need of fiducial

markers or any other modifications of the sample. However, they rely on the presence of features that remain visible over consecutive frames, which can be complicated due to blinking of the fluorophores. Fiducial tracking compensates the distortion of the SMLM localization map due to drift by tracking the sample movement during the experiment via fixed fiducial markers. The drift can then be corrected by subtracting the measured fiducial track from the obtained localization coordinates.[11,12] Using a tetrapod point-spread function (PSF) for imaging the fiducials allows us to track both their lateral and axial position and, hence, to correct the obtained localizations in all three dimensions.[16] The signal from the fiducial markers is typically recorded at the same frame rate as the signal from the fluorophore emitters.

In cryo-SMLM, however, this could be insufficient, as the low frame rate of down to 1 Hz[7] might lead to significant drifts already during the illumination of a single frame. The measured intensity pattern then may deviate substantially from that of a static emitter. Localization procedures using a maximum-likelihood estimator of the position, which assume a point-spread function (PSF) model without drift, can then become unstable. In the context of a multi-parameter fit, drift-induced distortions of the measured intensity pattern likely introduce errors in the localization.[17] To retain superresolution on the nanometer scale, it may, hence, be necessary to account for drift also in the fitting procedure. In this paper, we present a localization method for cryo-SMLM that accounts for distortions of the PSF due to sample drift directly in the fitting procedure. This approaches make nanometer precision feasible even in the case of very large sample drifts up to several hundred nanometers per frame.

We employ maximum-likelihood estimation for 2D-position and defocus using an astigmatic imaging model similar to Ref. 18. In order to account for sample drift in the fitting procedure, an estimate of the drift trajectory during the image acquisition time is required. Figure 1 illustrates the illumination protocol and the image acquisition and fitting procedure. While the sample of interest is excited and imaged during one frame, several subframes are recorded of the fiducial markers. Thus, the position of the fiducial markers can be tracked on a smaller timescale, and an estimate of the drift trajectory within the SMLM frame is obtained. This drift estimate is then incorporated into the maximum-likelihood fit of the sample PSF. Details about the image formation model and parameter estimation procedure are provided in the supplementary material.

If not mentioned otherwise, we assume in the following that we sample the drift at 25 uniformly spaced time steps during one frame. We refer to this sampling rate as the *trajectory sampling rate*. In the following simulations, we further assume that the position of fiducial markers at these time steps is known exactly. Later, we will incorporate localization errors to capture a more realistic scenario.

In the following figures, we show results for the localization precision σ_x and accuracy μ_x of the $x-$component for various simulation settings. The results for the y-component are similar and were omitted for clarity. We assumed an integrated signal photon count of 10^5 and Poissonian background noise with a standard deviation of 100 photons per pixel.

In Fig. 2, we compare the performance of our proposed fitting procedure including the drift trajectory against a fit that assumes only the centroid of the drift motion to be known. For convenience, we refer to these two types of fit as *dynamic fit* and *static fit*. We show the

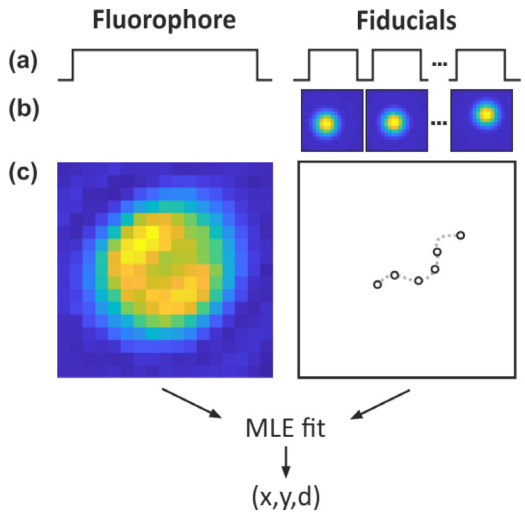

FIG. 1. Fitting procedure accounting for drift. The figure illustrates an overview of the experimental protocol assumed in the simulations and the fitting procedure taking into account the drift trajectory of the sample. During the recording of one frame of the sample, several subframes of fiducial markers are recorded. Panel (a) shows the illumination protocols for the imaged fluorophore (left) and the fiducial markers (right). The resulting PSF images are shown in panel (b) for the fiducials and panel (c) for the fluorophore. Localization of the fiducial markers yields an estimate of the drift trajectory [panel (c), right]. The gray line indicates the underlying ground truth drift trajectory, and the black circles show the estimated position of the fiducial marker at the sampled time points. The estimated drift trajectory is incorporated in the MLE fit of the sample PSF, yielding an estimate of lateral position (x, y) and defocus d.

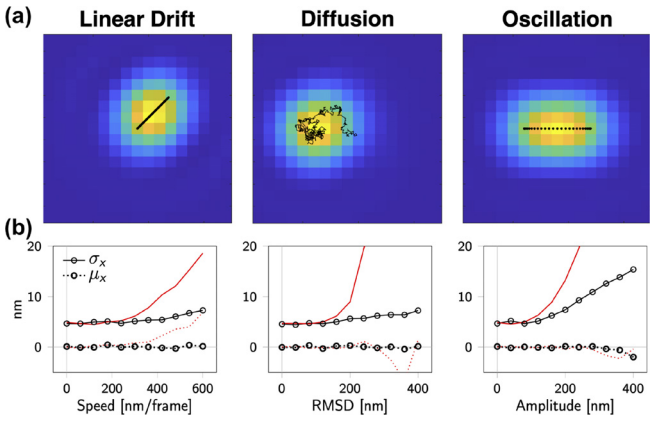

FIG. 2. Influence of drift on localization precision (static fit and dynamic fit). (a) PSF images in the case of linear drift with a speed of 400 nm/frame, diffusion with a root mean square deviation (RMSD) of 300 nm/ frame and oscillation with an amplitude of 300 nm (left to right). (b) Localization precision (solid line) and accuracy (dotted line). The red lines show results for a static fitting procedure that only assumes knowledge about the centroid of the drift motion (corresponding to standard fiducial correction). The black lines show results for the dynamic fit taking into account the drift trajectory. As localization algorithm we use maximum-likelihood estimation (MLE) with the PSF model described in the supplementary material. For each data point, we simulated fluorophores with random but fixed dipole orientations. Each data point represents the result of 1000 simulations.

results for fixed dipole emitters undergoing three different types of sample movement, either linear drift, diffusion, or oscillation. In the case of small sample movements, the dynamic and static fit show similar results. However, for large drifts, the dynamic fit yields superior fit results, showing stable localization results up to 600 nm for the linear drift and up to 400 nm root mean square deviation (RMSD) for diffusion. Only in the case of oscillation, the performance decreases slightly for large amplitudes but is still highly superior to the static fit.

Next, we examined the effect of dipole orientation on the performance of the localization procedure. In cryogenic conditions, the dipole of each emitter is fixed and the anisotropic emission pattern results in characteristic intensity patterns for each dipole orientation that may respond differently to sample drift. Figure 3 confirms this suspicion. The three panels show different assumed inclination angles of the fluorophore dipole ranging from $\theta = \pi/2$ (i.e., perpendicular to the optical axis) to $\theta = 0$ (i.e., parallel to the optical axis). We assume that the emitter undergoes linear drift along the image diagonal, as indicated by the black lines in panel (b). The doughnut-shaped intensity pattern associated with dipoles parallel to the optical axis ($\theta = 0$) is found to be more sensitive to large sample drifts.

Up to now, we only considered a trajectory sampling rate of either 1 or 25. In Fig. 4(a), we investigate the influence of a range of different sampling rates. We assume diffusion with a RMSD of 100 and 300 nm per frame. At a RMSD of 100 nm per frame, no gain in localization precision is achieved by increasing the sampling rate. However, in the case of the larger RMSD of 300 nm per frame,

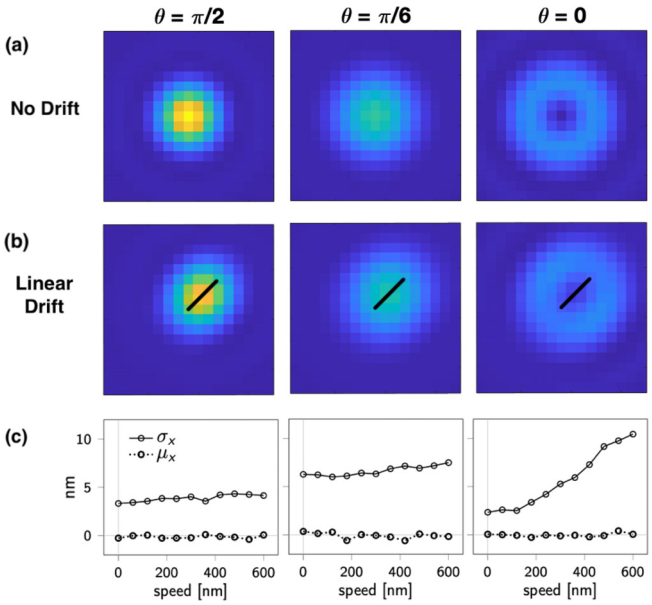

FIG. 3. Influence of inclination angle. Simulations were carried out assuming a linear drift of 0 − 600 nm and fixed inclination angles $\theta = \pi/2, \pi/6, 0$ (left to right). Row (a) shows intensity distributions of emitters not undergoing any drift. Row (b) shows the intensity distributions simulated from emitters undergoing linear drift with a speed of 400 nm per frame. The drift trajectory is indicated by a black line. Row (c) shows the localization precision (solid line) and bias (dotted line) when performing a dynamic fit with 25 trajectory sampling points. We assume a constant photon count of 10^5 that is independent of orientation. Each data point represents 500 simulations.

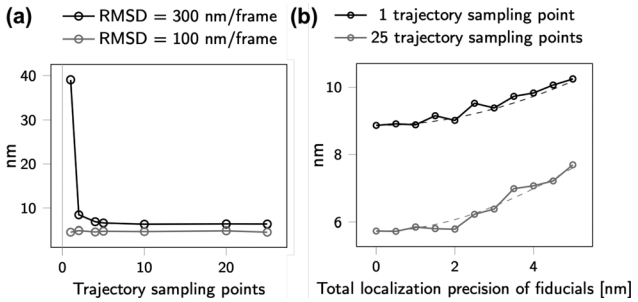

FIG. 4. Influence of fiducial trajectory parameters. (a) Number of trajectory sampling points. We show localization precision σ_x for diffusion with a RMSD of 100 and 300 nm per frame. The number of trajectory sampling points is varied from 1 to 25. The total localization precision of fiducials is set to 1 nm and is adjusted w.r.t. the number of trajectory sampling points. Each data point represents 2500 simulations. (b) Fiducial localization precision. Localization precision σ_x for samples undergoing a linear drift (with a speed of 400 nm/frame) during the image recording process, where only a noisy estimate of the motion is known. We show results for different values of the total fiducial localization precision between 0 (noise-free) and 5 nm, defined as the precision achieved with a trajectory sampling rate of 1. For a sampling rate of 25, the precision is adjusted accordingly, due to the overall constant photon budget being split up over 25 frames. Results shown without subsampling of the trajectory (black line) and with 25 trajectory sampling points (gray line). The dashed lines show the predicted precision. Each data point represents 1000 simulations.

the localization precision improves significantly when increasing the sampling rate to 4. Surprisingly, a further increase in the sampling rate was not found to yield any further improvements.

So far, we assumed that we have an error-free estimate of the sample drift. In reality, the positions of the fiducial markers can only be estimated with a certain nonzero precision. In Fig. 4(b), we investigated quantitatively how these errors in the drift trajectory deteriorate the localization precision of the sample fluorophores. For this, we vary the localization precision for the fiducial markers, σ_{fid} between 0 and 5 nm, corresponding to a photon count of approximately 10^4 (compare Ref. 19). First, we simulate trajectories recorded at a sampling rate of 1. As expected, the localization precision for the fluorophore, σ_x, scales with σ_{fid} according to $\sigma_x = \sqrt{\sigma_0^2 + \sigma_{\text{fid}}^2}$, where σ_0 is the localization precision for the fluorophore in the absence of trajectory noise. Next, we are interested whether a higher trajectory sampling rate improves the results. In practice, this implies a deteriorated localization precision σ_{fid}, since the overall photon budget for each fiducial marker is divided into several subframes. For example, a trajectory sampling rate of 25 results in a σ_{fid} that is deteriorated by a factor of 5 [cf. Eq. (5) in Ref. 20]. To facilitate the comparability of the two sampling rates, on the x-axis, we plot the total localization precision, which would be achieved if the total photon budget of the fiducial marker was recorded in a single frame. Interestingly, despite a fivefold deteriorated localization precision, we observe an improved localization precision for the single fluorophore, most likely since the full drift trajectory could now be considered in the analysis.

Finally, in Fig. 5, we examine the scenario where an emitter switches off during the image acquisition of a single frame. For the drift scenario, we choose linear drift with a speed of 200nm per frame. We assume the emitter to be active at the beginning of the recording of the frame and to switch off at a time point varying from 20% to 100%

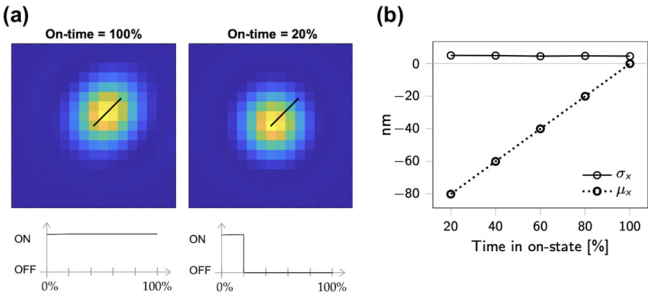

FIG. 5. Influence of off-switching of fluorophore during frame. We assume the fluorophore to be active at the beginning of the illumination, and to switch to the dark state after 20% to 100% of the illumination time. (a) Intensity patterns of two emitters undergoing identical linear drift. The emitter in the left image is continuously on, while the emitter in the right image switches to the off-state after 20% of the frame recording time. (b) Arising localization precision σ_x and accuracy μ_x for a drift of 200nm per frame. Each data point represents 1000 simulations.

of the total recording time for the single frame. As expected, this transition introduces a very large localization bias.

So far we only considered sample drift in the xy-plane. However, the sample might drift in axial direction relative to the objective, resulting in defocusing. Typically, axial drift is corrected by employing a focus-hold system. To test the limits of our method, we investigated the effect of substantial axial drifts that might appear in the absence of such a system. In supplementary material Fig. S1, we test the robustness of our method in the presence of linear axial drift with a speed of up to 400 nm per frame. While the localization precision remains below 6nm, the axial drift introduces a bias of up to 3 nm in x-direction at an axial drift of 400 nm per frame. If an estimate of the full 3D drift trajectory is available, this information can be included in the fitting algorithm. In supplementary material Fig. S2, we repeat the same simulations as in supplementary material Fig. S1 but utilize knowledge about the 3D trajectory in the fitting procedure. This allows us to avoid localization bias and improves localization errors. Overall, the localization procedure is robust w.r.t. (linear) axial drift.

To summarize, in this paper, we investigated the impact of sample drift on the determination of fixed dipole positions from SMLM data. We considered an astigmatic PSF model for localization and simulation parameters typical for cryo-SMLM data. The commonly used strategy of imaging the drift trajectory with the same frame rate as the sample was found to be sufficient to achieve nanometer precision in the case of low to moderate sample drift. This method was found to be surprisingly stable even with drift magnitudes of up to 200nm. However, for very large drifts, a significant degradation of the localization precision was detected, indicating the necessity of more sophisticated correction.

Sampling the drift trajectory at a higher rate was found to restore a localization precision that is similar to what could be achieved without drift, retaining nanometer precision even in the presence of drift of several hundred nanometers. This was showcased for three different types of drift that are experimentally most relevant: linear drift, diffusion, and oscillation. For the rather large magnitudes of drift considered here, a trajectory sampling rate of 4 was determined to be sufficient. Along this line, a conceptually similar approach to the one explored here has been reported in Ref. 7. Therefore, the drift correction is preceded by a binning step to improve the SNR. A key difference is the way in which the measured drift enters the method and the choice of the PSF model. In Ref. 7, an elliptical Gaussian PSF model was assumed and the drift was subtracted from the data before fitting. In contrast, here we use a full vectorial PSF model and leave the data unaltered, while incorporating the measured drift into the PSF model for fitting.

The photostability of the fluorophore within a frame is important for our method to yield accurate results. Off-switching of an emitter within the acquisition of a single frame was found to induce a substantial localization bias. In an experiment, however, the typical on-time of a fluorophore exceeds the duration of a single frame, and the fluorophore will be imaged throughout multiple consecutive frames. Hence, this issue can be avoided by discarding the first and last frame, in which the fluorophore was detected, from the analysis. Alternatively, the time point of on- or off-switching can be estimated from the intensity in the affected frame compared to the intensity of the on-frames.

In particular for large drifts, the analysis region for the fitting needs to be chosen large enough such that it contains the entire signal. This requires sufficient spatial separation of individual emitter signals and, in particular, no signal overlap.

All in all, we have demonstrated that the standard fiducial correction of sample drift achieves good results for low to moderate levels of sample drift. In the case of very large drifts, increasing the sample rate of the fiducials and accounting for the drift trajectory in the fitting procedure restore nanometer precision, allowing for very long image acquisition times for individual frames in cryo-SMLM.

See the supplementary material for the detailed information about the image formation model, data simulation, and parameter estimation, as well as the supplementary Figs. S1 and S2.

F.H., S.H., and R.R. were funded by the Austrian Science Fund (FWF): F6805-N34. M.C.S., M.L., and G.J.S. were funded by the Austrian Science Fund (FWF): F6809-N34. M.C.S. was additionally supported by Howard Hughes Medical Institute, Janelia Research Campus.

AUTHOR DECLARATIONS

Conflict of Interest

The authors have no conflicts to disclose.

Author Contributions

Fabian Hinterer: Conceptualization (equal); Formal analysis (equal); Investigation (equal); Methodology (equal); Software (equal); Validation (equal); Visualization (equal); Writing – original draft (equal); Writing – review & editing (equal). **Magdalena C. Schneider:** Conceptualization (equal); Formal analysis (equal); Investigation (equal); Methodology (equal); Software (equal); Validation (equal); Visualization (equal); Writing – original draft (equal); Writing – review & editing (equal). **Simon Hubmer:** Conceptualization (equal); Supervision (equal); Writing – review & editing (equal). **Montserrat López Martínez:** Conceptualization (equal); Writing – original draft (equal); Writing – review & editing (equal). **Ronny Ramlau:** Conceptualization (equal); Funding acquisition (equal); Supervision (equal); Writing – review & editing (equal). **Gerhard J. Schütz:** Conceptualization (equal); Funding acquisition (equal); Investigation (equal); Supervision (equal); Writing – original draft (equal); Writing – review & editing (equal).

DATA AVAILABILITY

The data that support the findings of this study are available from the corresponding authors upon reasonable request. The data that support the findings of this study are openly available in GitHub at https://github.com/schuetzgroup/localizationFixedDipoles-motionFit, Ref. 21.

REFERENCES

[1]M. J. Rust, M. Bates, and X. Zhuang, "Sub-diffraction-limit imaging by stochastic optical reconstruction microscopy (STORM)," Nat. Methods **3**, 793–795 (2006).

[2]B. Huang, W. Wang, M. Bates, and X. Zhuang, "Three-dimensional super-resolution imaging by stochastic optical reconstruction microscopy," Science **319**, 810–813 (2008).

[3]S. Hess, T. Girirajan, and M. Mason, "Ultra-high resolution imaging by fluorescence photoactivation localization microscopy," Biophys. J. **91**, 4258–4272 (2006).

[4]R. Kaufmann, C. Hagen, and K. Grünewald, "Fluorescence cryo-microscopy: Current challenges and prospects," Curr. Opin. Chem. Biol. **20**, 86–91 (2014).

[5]W. Li, S. C. Stein, I. Gregor, and J. Enderlein, "Ultra-stable and versatile wide-field cryo-fluorescence microscope for single-molecule localization with sub-nanometer accuracy," Opt. Express **23**, 3770–3783 (2015).

[6]M. Shang, Z.-L. Huang, and Y. Wang, "Influence of drift correction precision on super-resolution localization microscopy," Appl. Opt. **61**, 3516–3522 (2022).

[7]P. D. Dahlberg, A. M. Sartor, J. Wang, S. Saurabh, L. Shapiro, and W. Moerner, "Identification of PAmKate as a red photoactivatable fluorescent protein for cryogenic super-resolution imaging," J. Am. Chem. Soc. **140**, 12310–12313 (2018).

[8]S. Coelho, J. Baek, M. S. Graus, J. M. Halstead, P. R. Nicovich, K. Feher, H. Gandhi, J. J. Gooding, and K. Gaus, "Ultraprecise single-molecule localization microscopy enables in situ distance measurements in intact cells," Sci. Adv. **6**, eaay8271 (2020).

[9]A. Pertsinidis, Y. Zhang, and S. Chu, "Subnanometre single-molecule localization, registration and distance measurements," Nature **466**, 647–651 (2010).

[10]B. Liu, Y. Xue, W. Zhao, Y. Chen, C. Fan, L. Gu, Y. Zhang, X. Zhang, L. Sun, X. Huang, W. Ding, F. Sun, W. Ji, and T. Xu, "Three-dimensional super-resolution protein localization correlated with vitrified cellular context," Sci. Rep. **5**, 13017 (2015).

[11]S. H. Lee, M. Baday, M. Tjioe, P. D. Simonson, R. Zhang, E. Cai, and P. R. Selvin, "Using fixed fiduciary markers for stage drift correction," Opt. Express **20**, 12177–12183 (2012).

[12]H. Ma, J. Xu, J. Jin, Y. Huang, and Y. Liu, "A simple marker-assisted 3D nanometer drift correction method for superresolution microscopy," Biophys. J. **112**, 2196–2208 (2017).

[13]A. Balinovic, D. Albrecht, and U. Endesfelder, "Spectrally red-shifted fluorescent fiducial markers for optimal drift correction in localization microscopy," J. Phys. D: Appl. Phys. **52**, 204002 (2019).

[14]M. J. Mlodzianoski, J. M. Schreiner, S. P. Callahan, K. Smolková, A. Dlasková, J. Šantorová, P. Ježek, and J. Bewersdorf, "Sample drift correction in 3D fluorescence photoactivation localization microscopy," Opt. Express **19**, 15009–15019 (2011).

[15]Y. Wang, J. Schnitzbauer, Z. Hu, X. Li, Y. Cheng, Z.-L. Huang, and B. Huang, "Localization events-based sample drift correction for localization microscopy with redundant cross-correlation algorithm," Opt. Express **22**, 15982–15991 (2014).

[16]A.-K. Gustavsson, R. P. Ghosh, P. N. Petrov, J. T. Liphardt, and W. Moerner, "Fast and parallel nanoscale three-dimensional tracking of heterogeneous mammalian chromatin dynamics," Mol. Biol. Cell **33**, ar47 (2022).

[17]H. Deschout, K. Neyts, and K. Braeckmans, "The influence of movement on the localization precision of sub-resolution particles in fluorescence microscopy," J. Biophotonics **5**, 97–109 (2012).

[18]F. Hinterer, M. C. Schneider, S. Hubmer, M. López-Martinez, P. Zelger, A. Jesacher, R. Ramlau, and G. J. Schütz, "Robust and bias-free localization of individual fixed dipole emitters achieving the Cramér Rao bound for applications in cryo-single molecule localization microscopy," PLoS One **17**, e0263500 (2022).

[19]C. S. Smith, N. Joseph, B. Rieger, and K. A. Lidke, "Fast, single-molecule localization that achieves theoretically minimum uncertainty," Nat. Methods **7**, 373–375 (2010).

[20]R. Thompson, D. Larson, and W. Webb, "Precise nanometer localization analysis for individual fluorescent probes," Biophys. J. **82**, 2775–2783 (2002).

[21]F. Hinterer and M. C. Schneider (2023). "localizationFixedDipoles-motionFit," GitHub. https://github.com/schuetzgroup/localizationFixedDipoles-motionFit